

Published: August 31, 2023

Citation: Miura K and Iwashita T, 2023. Simultaneous Evaluation of Stiffness and Histology in Orthopedic Diseases Using Scanning Acoustic Microscope, Medical Research Archives, [online] 11(8).
<https://doi.org/10.18103/mra.v11i8.4302>

Copyright: © 2023 European Society of Medicine. This is an open-access article distributed under the terms of the Creative Commons Attribution License, which permits unrestricted use, distribution, and reproduction in any medium, provided the original author and source are credited.

DOI
<https://doi.org/10.18103/mra.v11i8.4302>

ISSN: 2375-1924

RESEARCH ARTICLE

Simultaneous Evaluation of Stiffness and Histology in Orthopedic Diseases Using Scanning Acoustic Microscope

Katsutoshi Miura^{1*}, Toshihide Iwashita¹

¹ Department of Regenerative & Infectious Pathology, Hamamatsu University School of Medicine

*Correspondence author: kmiura.hama.med@gmail.com

ABSTRACT

Organs with different levels of stiffness support the musculoskeletal system. Light microscopy cannot evaluate organ stiffness, whereas scanning acoustic microscopy (SAM) discriminates stiffness based on speed-of-sound (SOS) because sound waves pass faster in stiffer tissues. This study aimed to evaluate SOS imaging for orthopedic diseases using formalin-fixed paraffin-embedded sections. SOS imaging in SAM uses unstained light microscopic (LM) sections to prevent the bias of staining variation. Digital SOS values are comparable in different organ components and diseases.

Mouse organs with the lowest mean SOS values included the adipose tissue, bone marrow, calcified cartilage, and nucleus pulposus; those with intermediate values included hyaline cartilages, osteoid, skeletal muscles, cortical and trabecular bones, and ligaments; and those with the highest values comprised fibrocartilages of the vertebral disc and meniscus. Water contents and delipidating procedures decreased SOS values. Collagenous density and arrangement affected higher SOS values. The trabecular bones of mice were thinner and showed significantly lower values of SOS than those of humans.

Various orthopedic diseases and disorders displayed the characteristic SOS images. In osteoporosis, the trabecular bone becomes thin with lower SOS, indicating lesser stiffness to cause fractures. Comparison of woven and lamellar bones revealed that woven bones with lower SOS had lesser stiffness to fracture. Changes in SOS values indicated intramembranous bone formation. The trabecular bone develops from the connective tissues with an abrupt increase in SOS values. The regenerating process of bone fractures was monitored using SOS images, in which the granulation tissues transformed into calli in the osteoid to grow a new mineralized bone. The stiffness increased in phases, which appeared in SOS values.

Although several methods have been used to visualize the stiffness of biological tissues, SAM only needs 10- μ m unstained slides and can simultaneously compare mechanical stiffness and histology. SOS images provide informative mechanical alterations of the bone, cartilage, and connective tissues to assess the status and diagnose a disorder.

Introduction

Bones are rigid organs supporting the body, storing minerals, and producing blood cells. Specimens of various bone diseases are subjected to pathological examination for accurate diagnosis, and decalcified sections are typically used for routine pathological diagnosis. However, this decalcification procedure makes differentiating mineralized and unmineralized areas difficult. Hence, special staining^{1,2} or fixatives³ are required to effectively determine mineralized bones, unmineralized bones (osteoid), and cartilages after decalcification.

Diagnosing orthopedic diseases such as osteoporosis, osteoarthritis, and neoplastic bone requires histological analysis of structural alteration, including the bones, cartilage, and surrounding connective tissues. Furthermore, assessing the process of bone formation, remodeling, fracture healing, and articular cartilage alterations requires histological differentiation of these structures.

The bones, osteoid, cartilages, and peripheral connective tissues have different textures and stiffness. Despite the need for mechanical information about these components, light microscopy (LM) cannot determine the degree of tissue stiffness.

Scanning acoustic microscopy (SAM)⁴⁵ is used to create histological images similar to LM, and it can differentiate tissue stiffness based on the speed-of-sound (SOS) values because the stiffer the tissue, the higher the SOS⁶⁷.

The relationship between the SOS and the elastic bulk modulus of a liquid-like medium can be represented using the Newton–Laplace equation as follows⁸:

$$c = (K / \rho)^{1/2}$$

where c is the SOS, K is the bulk modulus of elasticity, and ρ is the density.

Thus, the SOS increases with material stiffness (the resistance of an elastic body to deformation by an applied force) but decreases with density. As the thin sections were soaked in water during the measurement period, the average soft-tissue density was nearly 1 g/cm³⁹, and the SOS through the soft tissues was strongly correlated with their stiffness.

This study evaluates whether SAM can examine orthopedic diseases using routine decalcified formalin-fixed paraffin-embedded (FFPE) sections. SAM has been used to assess bone sections for research and clinical purposes^{10,11,12}. Fresh bone

samples are best to evaluate bone and cartilage quality. However, flat, smooth surface samples are mandatory for high-frequency acoustic inspection due to regular reflection of the sound waves¹⁰. For sample durability and easy sample preparation, methods of cutting embedded tissues after fixation have advantages and have been used in previous SAM studies of bone.

Routine FFPE sections have not been used for SOS imaging because many artificial events affect original tissue properties. This study shed light on the availability of routine FFPE sections for histological and functional analysis of orthopedic disorders. Even FFPE sections show characteristic images with various stiffness in different conditions.

Materials and Methods

PREPARATION OF MOUSE BONE SPECIMENS

Adult male mice (8 weeks old, Japan SLC, Hamamatsu) were kindly provided by Dr. Y. Enomoto from Regenerative & Infectious Pathology, Hamamatsu University School of Medicine. Bone tissues were resected after decapitation under deep anesthesia and fixed in a 10% buffered formalin solution for 4 days. After fixation, the bones were soaked in 0.5 mol/l ethylenediaminetetraacetic acid (EDTA) solution (Fujifilm Wako chemicals, Tokyo, Japan) or Plank Rychlo solution (Fujifilm Wako chemicals) for 2 days and 1 day, respectively, for decalcification. Then, after washing with phosphate-buffered saline solution, the specimen was processed into ordinary paraffin sections on the glass slide. The 10- μ m-thick flat sections were made for SAM, whereas 4- μ m-thick sections were sliced for LM.

HUMAN SPECIMEN PREPARATION

The study protocol conformed to the ethical guidelines of the Declaration of Helsinki and was approved by the ethical committee of the Hamamatsu University School of Medicine (approval no. 19-180). Stored pathology paraffin blocks without a link to the patient's identity were used for this study. All procedures were conducted according to approved ethical committee guidelines and regulations. All bone samples were fixed in 10% buffered formalin solution and decalcified in 0.5 mol/l EDTA solution for the biopsy specimen and Plank Rychlo solution for large specimens. After decalcification, the tissues were embedded in paraffin and cut into flat sections.

SCANNING ACOUSTIC MICROSCOPIC (SAM) OBSERVATIONS

Bone specimens were examined using the SAM system (AMS-50AI; Honda Electronics, Toyohashi, Aichi, Japan) with a central frequency of 320 MHz

and a lateral resolution of approximately 4.0 μm (Figure 1)^{5, 13, 14}. The transducer was excited with a 2-ns electrical pulse to emit an acoustic pulse¹⁵. Samples were placed above the transducer, and distilled water at 20 °C was used for coupling the fluid between the transducer and specimen. The transducer was used to both transmit and receive

the signal. Waveforms reflected from the surface and bottom of the sample were compared to measure the SOS and thickness of each point. The waveform from a glass surface without the selection was considered the reference, with SOS only through the water, and 1,495 m/s was used as the standard value.

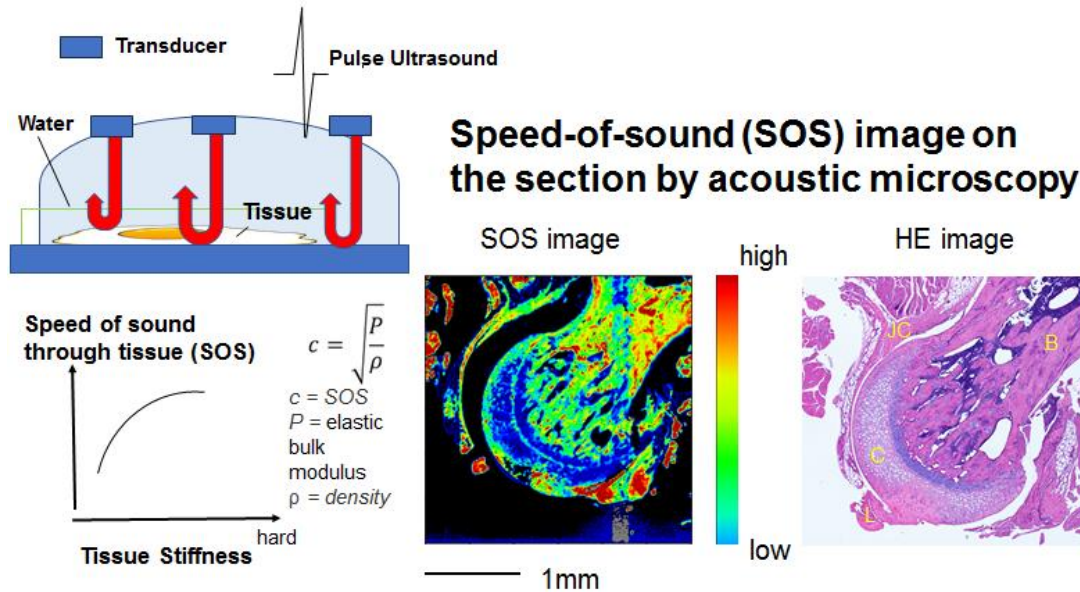


Figure 1. Principles of speed-of-sound (SOS) observation

Sound waves irradiated from the transducer hit and returned from the surface and bottom of the specimen. The time delay of the wave from the bottom depends on the SOS through the section. The reference SOS value is 1,495 m/s through water, obtained by the wave outside the section. Because SOS is higher from stiffer portions, the SOS image indicates the section stiffness map. The SOS image with the corresponding LM image in HE stains is an example. B; Trabecular bone, C; articular cartilage, JC; joint capsule, L; ligament

LIGHT MICROSCOPIC OBSERVATION

As a reference, light microscopic slides near the SAM sections were prepared to compare and identify the cartilage, osteoid, bones, and surrounding connective tissues. The slides were stained in hematoxylin and eosin (HE).

STATISTICAL ANALYSES

The means and standard deviations (SD) of SOS values were calculated from at least five areas per slide structure. The box plot shows the average (diamond), median (horizontal line), and interquartile range. Vertical bars indicate the 5th and 95th percentiles. A one-way analysis of variance was used to determine if there was a difference in the average SOS values. A p -value of <0.05 was considered to indicate statistical significance for all analyses.

Results

SPEED-OF-SOUND VALUES OF THE MUSCULOSKELETAL SYSTEM

Figures 2, 3, and 4 show SOS images of the mouse

hip, knee, and vertebral joints. SOS images displayed almost the exact resolution as LMs. Cartilages, osteoid, calcified bones, ligaments, meniscus, bone marrow, and adipose tissues showed intrinsic SOS values corresponding to palpable hardness to support mechanical stiffness. From the SOS images, three groups were divided according to the SOS values. The lowest group consisted of the adipose tissue, bone marrow, and calcified cartilage, shown in blue in the SOS image. The intermediate group includes hyaline cartilages of the meniscus and joint, osteoid, skeletal muscles, cortical and trabecular bones, and ligaments in the green to yellow color in the SOS images. The highest group was composed of fibrocartilages of the vertebral disc and meniscus, shown in red in the SOS image. Intra-articular space, cartilage, and the facing ligament had almost the same SOS values. In endochondral ossification, SOS values gradually increased from the cartilage to the osteoid following the calcified bone.

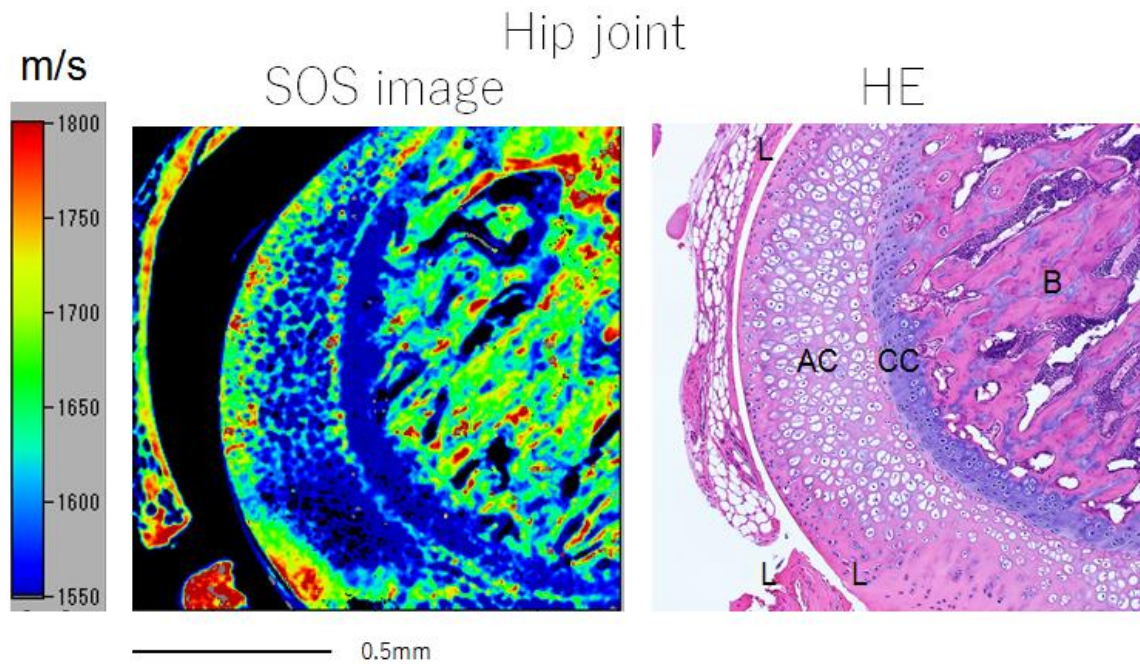


Figure 2. Speed-of-sound (SOS) and light microscopic images of the mouse hip joint

The femoral head consists of the surface of the hyaline cartilage and deeper cancellous bone. The ligament covers the head. The SOS values of the cartilage are lower than that of the trabecular bone. The bluish band in HE refers to a calcifying cartilage zone. In trabecular bones, the peripheral lower SOS portion is the unmineralized bone (osteoid), whereas the higher SOS portion at the center is the calcified bone. B; trabecular bone, AC; articular hyaline cartilage, CC; calcified cartilage, L; ligament

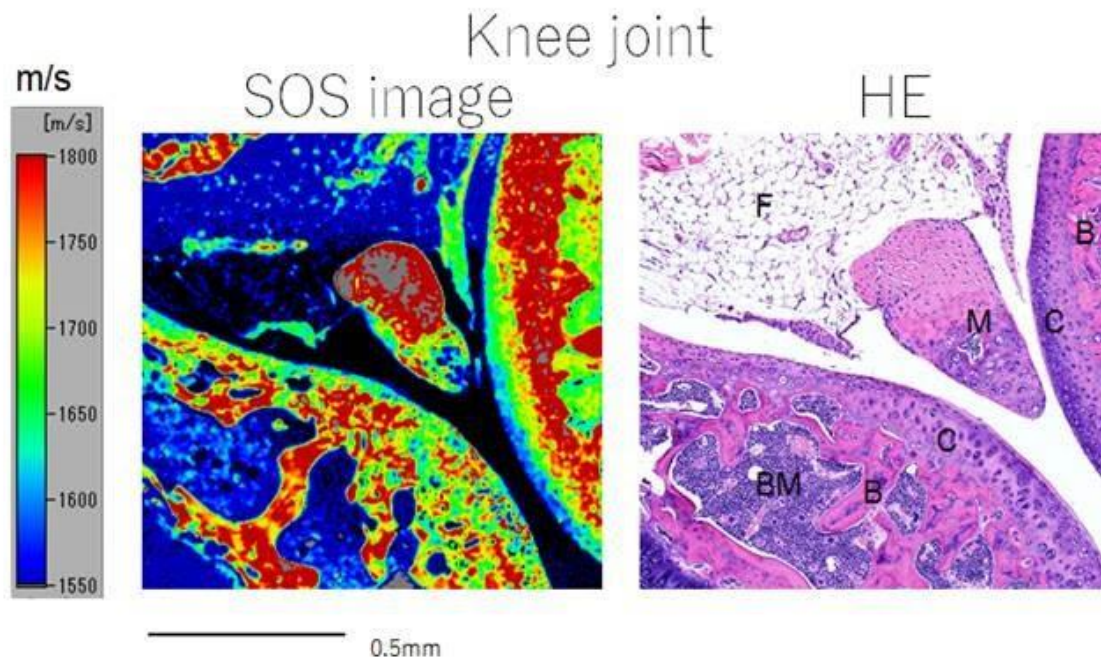


Figure 3. Speed-of-sound (SOS) and light microscopic images of the mouse knee joint

Surface hyaline cartilages show lower SOS zones than deeper trabecular bones. The joint meniscus comprises two parts: the fibrocartilage with a higher SOS and the hyaline cartilage with a lower SOS value, facing the joint cartilage with almost the same SOS value. Other structures, including the bone marrow and joint adipose tissues, display much lower SOS areas. B; trabecular bone, C; hyaline cartilage, M; meniscus, BM; bone marrow, F; adipose tissue

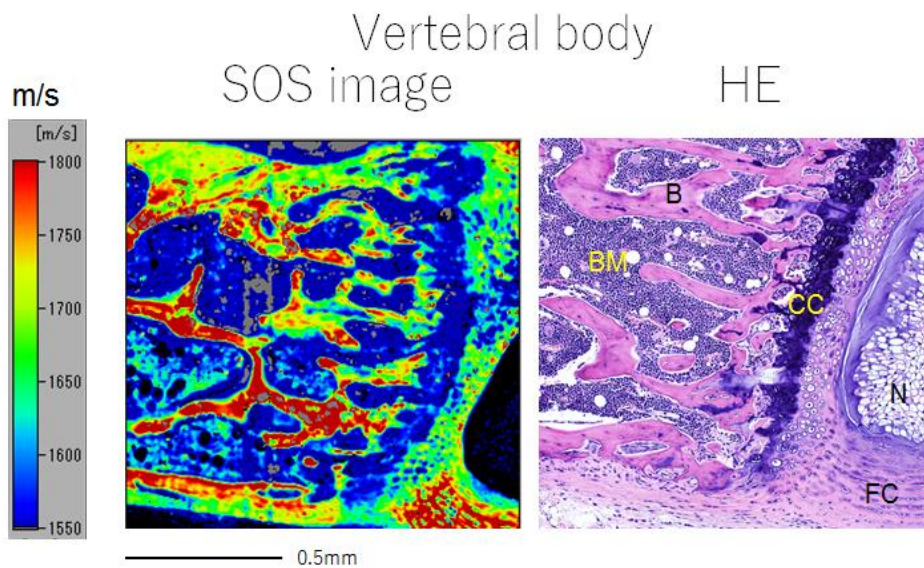


Figure 4. Speed-of-sound (SOS) and light microscopic images of the mouse vertebral joint

The vertebral disc of the fibrocartilage with central nucleus pulposus shows lower SOS than the trabecular bone. The calcifying cartilage zone displays a significantly lower SOS value, whereas the trabecular bone increases SOS values from the cartilage. The trabecular bone near the cartilage is an uncalcified osteoid with a slightly lower SOS value. The trabecula gradually alters to a higher SOS area corresponding to the calcified bone. FC; fibrocartilage, N; nucleus pulposus, CC; calcified cartilage, B; trabecular bone, BM; bone marrow

STATISTICAL ANALYSIS OF SPEED-OF-SOUND VALUES IN THE MOUSE MUSCULOSKELETAL SYSTEM

Organs of the mouse musculoskeletal system were lined up from left to right according to the average SOS value (Figure 5A, Table 1). SOS values were compared among hyaline cartilages consisting of the articular and meniscus cartilages, dense fibrocartilages including the vertebral discs and meniscus cartilages, osteoids, and decalcified bones (Fig 5B, Table 2). The hyaline cartilages and osteoids had significantly lower SOS values than the decalcified bones and fibrocartilages ($p < 0.001$). The fibrocartilage showed the most outstanding values compared with the other components ($p < 0.001$).

SPEED-OF-SOUND IMAGES OF THE FRACTURED BONE CALLUS IN HUMAN SPECIMENS

Fracture regeneration begins from immature granulation tissues to form a bridging callus. The granulation tissue with low SOS gradually altered the callus with higher SOS (Figure 6). The callus displayed low SOS at the periphery and higher SOS in the center, corresponding to calcified portions. The mean SOS values and SD of the granulation tissue, callus osteoid, and callus bone were 1551.9 ± 37.0 , 1812.5 ± 52.3 , and 2031.2 ± 71.9 m/s ($n = 10$ each), respectively, with significant differences ($p < 0.001$).

Table 1: Speed-of-sound values of mouse organs in the musculoskeletal system

	Adipose tissue	Bone marrow	Calcified cartilage	Meniscus hyaline	Osteoid	Articular cartilage	Skeletal muscles	Ligament	Cortical bone	Trabecular bone	Disc fibrocartila	Meniscus fibrocartila
n	5	15	25	9	50	30	30	5	17	15	15	12
Average m/s	1512.5	1527.8	1547.3	1675.9	1692.4	1692.5	1733.9	1746.5	1740.8	1757.3	1843.4	1904.5
SD	15.06	33.65	38.13	24.44	48.60	83.55	101.33	21.45	63.83	52.83	92.91	52.07

Table 2: Comparison of speed-of-sound values among mouse cartilage, osteoid, and fibrocartilage

	Hyaline cartilage	Osteoid	Calcified bone	Fibrocartilage
n	38	50	32	27
Average m/s	1681.1	1692.4	1748.5	1870.6
SD	57.88	48.60	58.59	82.19

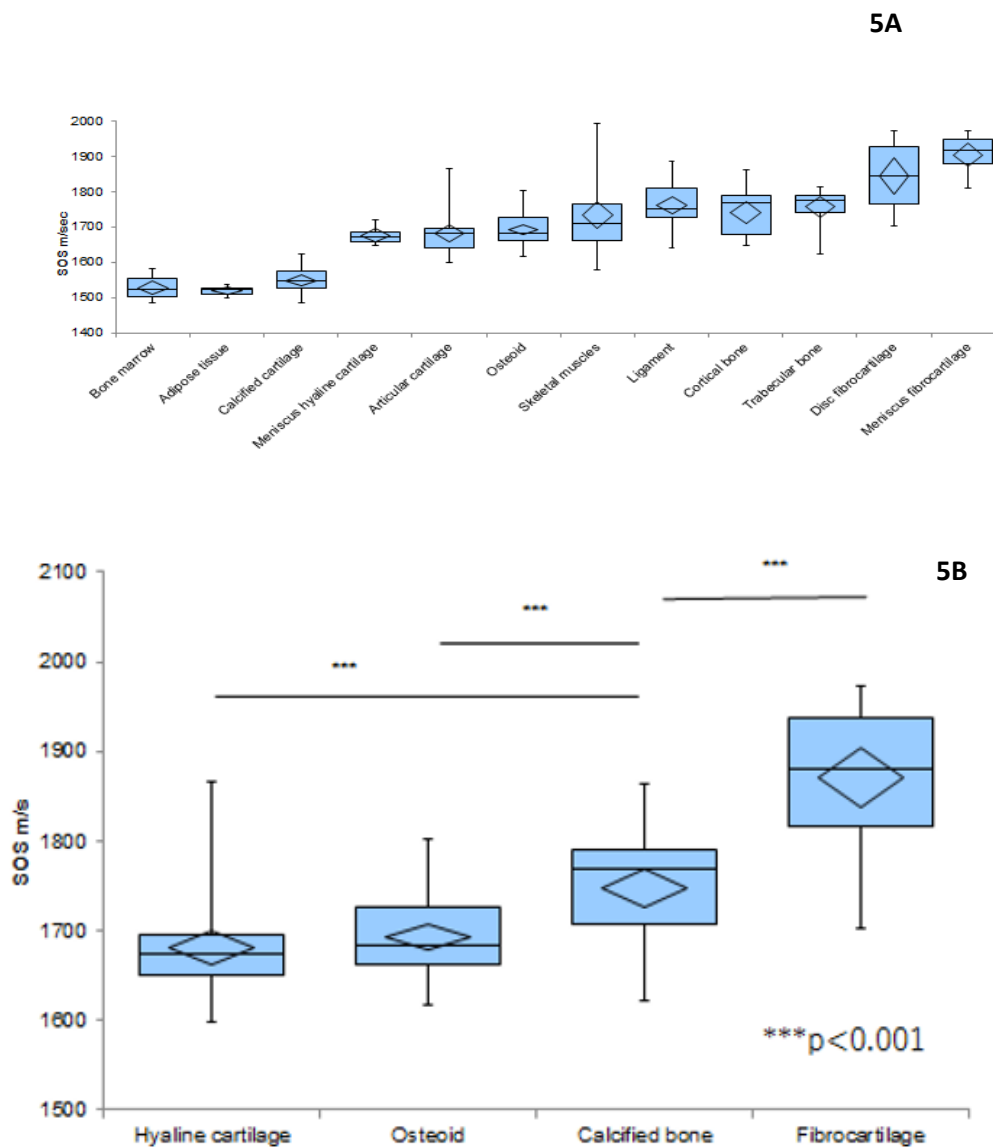


Figure 5. Comparison of speed-of-sound (SOS) values of the musculoskeletal system

A: Each organ of the musculoskeletal system, **B:** comparison among the cartilage, osteoid, and bone. The box plot compared SOS values among the musculoskeletal system organs. The box plot shows the mean (diamond), median (horizontal line), and interquartile range. Vertical bars indicate the 5th and 95th percentiles. In B, the hyaline cartilage consisted of articular and meniscus cartilage. The osteoid were unmineralized bones, the calcified bones were composed of cortical and trabecular bones, and the fibrocartilages contained vertebral disc and meniscus cartilages.

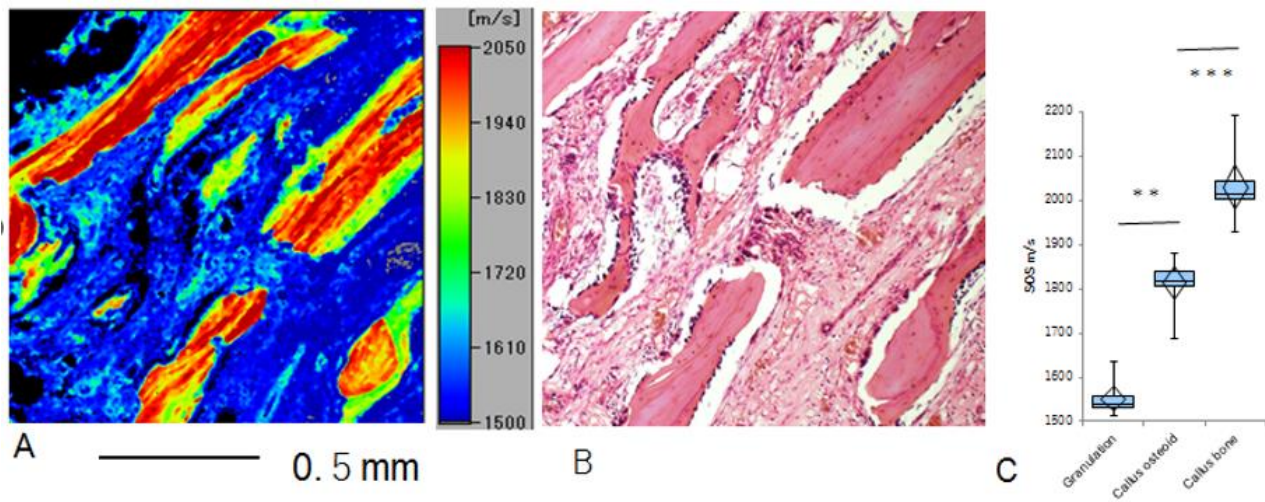


Figure 6. Callus of the femoral fracture bone

The callus is formed in the bone granulation tissues. The callus margins are noncalcified osteoid, whereas the center corresponds to a calcified bone. The sound velocity value is higher in the center. The granulation tissues between the callus show significantly lower SOS values. The average SOS values among the granulation tissue, callus osteoid, and callus bone show significant differences ($p < 0.001$). A; SOS image, B; HE image, C; Box plot of SOS values

SPEED-OF-SOUND IMAGES OF THE PERIOSTEUM WITH THE LIGAMENT

The ligament of thick collagen bundles is attached to the iliac bone periosteum. The outer fibrous layer of the periosteum, where the attached ligament showed high SOS values (2106.5 ± 64.98 m/s, $n = 10$) as trabecular bones (2098.2 ± 59.35 m/s, $n =$

10) (Figure 7). The SOS values of the inner layer were lower (1730.0 ± 45.12 m/s, $n = 10$), with almost the same values as the ligaments (1732.1 ± 48.94 m/s, $n = 10$). Bone marrows consisting of blood and fat cells showed significantly low SOS values.

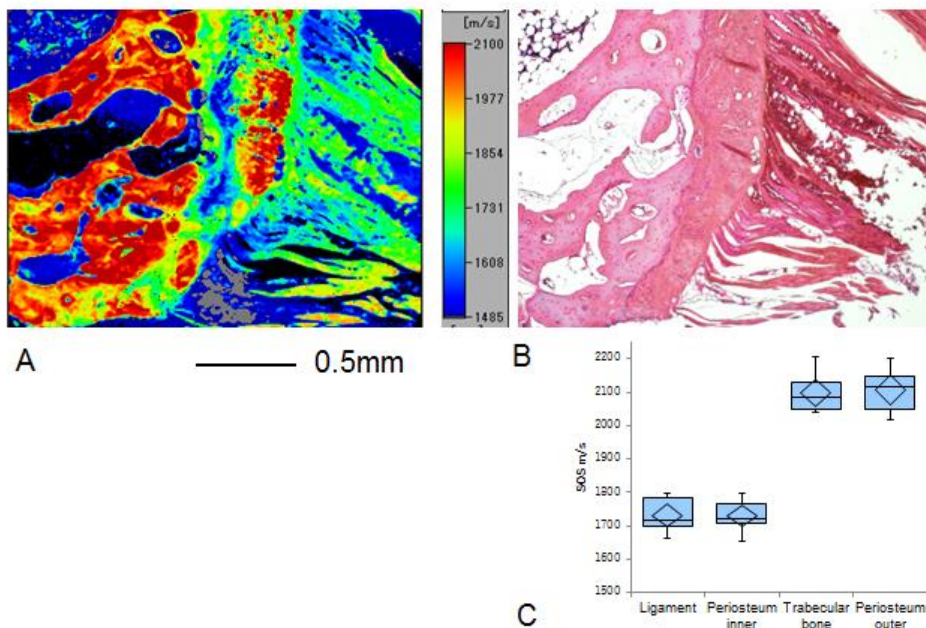


Figure 7. Iliac periosteum

Ligaments are attached to the right side of the thick fibrous periosteum, and the bone is formed on the left side. The outer fibrous periosteum displays high SOS values (2106.5 ± 64.98 m/s), similar to trabecular bones (2098.2 ± 59.35 m/s). The inner periosteum has a lower SOS value (1730.0 ± 45.12 m/s), almost the same as that of ligaments (1732.1 ± 48.94 m/s). A; SOS image, B; HE image, C; Box plot of SOS values

SPEED-OF-SOUND ALTERATION IN MEMBRANOUS OSSIFICATION

Membranous ossification occurs in immature connective tissues. Calcified bones with higher SOS values (1975.5 ± 107.6 m/s) abruptly appeared from the connective tissues with much lower SOS (1590.8 ± 35.9 m/s) (Figure 8). The SOS values were significantly different ($p < 0.001$).

SPEED-OF-SOUND OF NEOPLASTIC LESIONS

In fibrous dysplasia, the bone marrow is replaced by fibrous tissue. The trabecular bone consisted of woven bones with irregular reticules that showed lower SOS (1800 ± 34.78 m/s, $n = 10$) compared to lamellar bones (Figure 9).

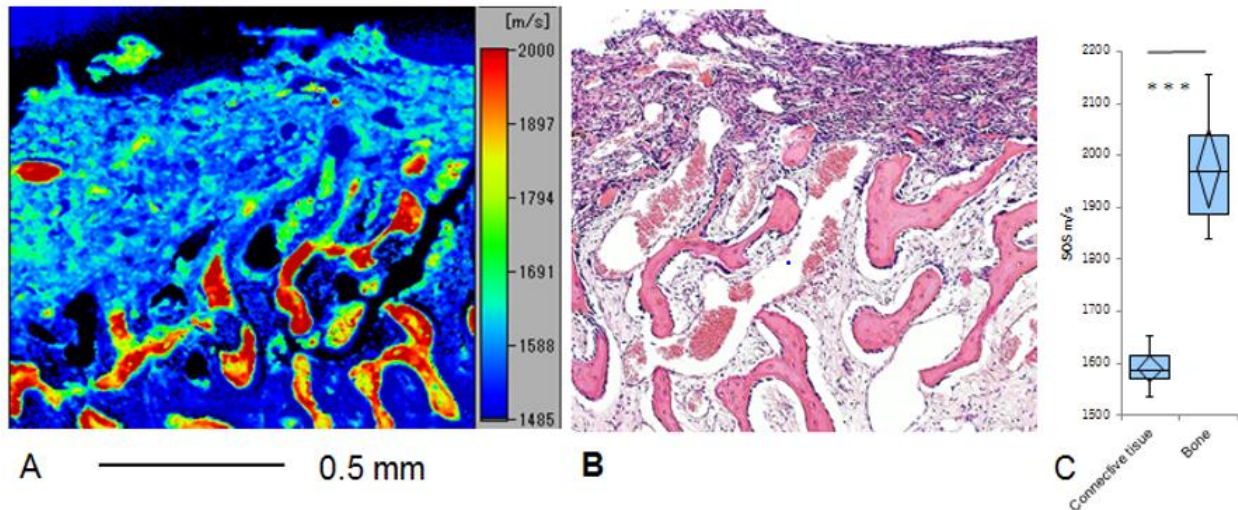


Figure 8. Membranous ossification of the rib

The bone is formed from membranous connective tissue. Sound velocity rapidly increases from the connective tissues (1590.8 ± 35.9 m/s) to the bones (1975.5 ± 107.6 m/s). The values between them show significant differences ($p < 0.001$). A; SOS image, B; HE image, C; Box plot showing SOS values of connective tissues and bone

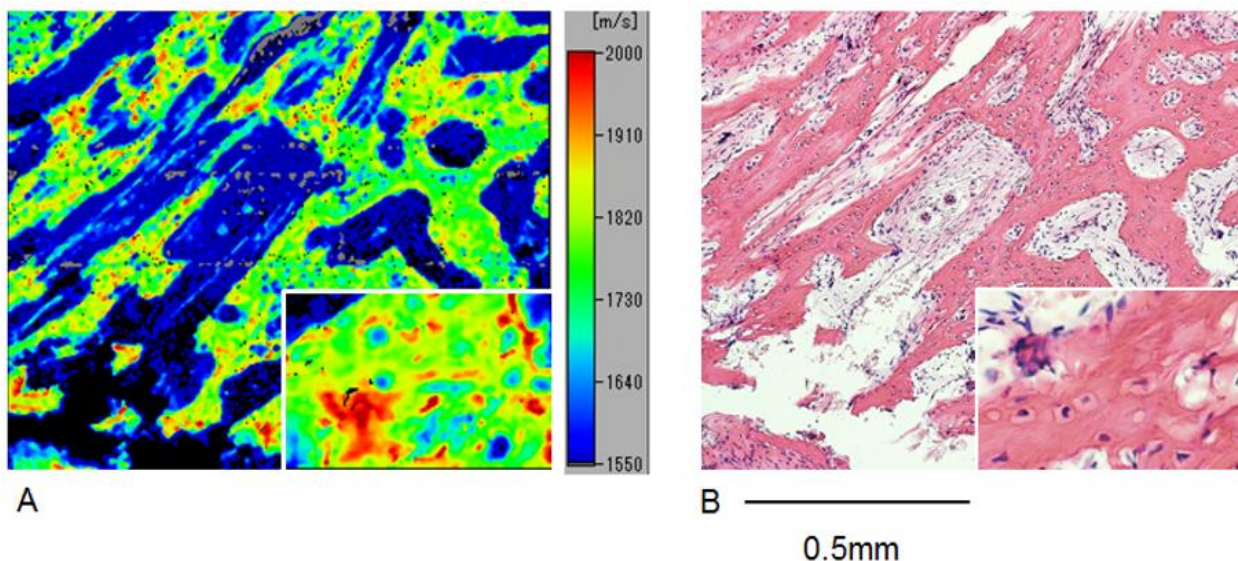


Figure 9. The woven bone of fibrous dysplasia

In fibrous dysplasia, the trabecular bone consisting of irregular reticules has lower SOS values (1800 ± 34.78 m/s) compared with calcified bone, causing the fracture in this case. Inlet: larger magnification of trabecular bone, A; SOS image, B; HE image

Osteosarcoma produces osteoid and woven bones with irregular shapes. SOS values greatly varied depending on the location (Figure 10).

COMPARISON OF CANCELLOUS TRABECULAR BONES BETWEEN OSTEOPOROSIS AND HEALTHY BONES

The osteoporotic bones consisted of thin sparse trabeculae compared to normal thick trabeculae (Figure 11). The SOS values of osteoporosis were lower (1941 ± 45.11 m/s, $n = 19$) with poor collagen fibers. Conversely, those of normal bones were higher (2005.4 ± 42.13 m/s, $n = 19$) with thick, rich collagens. Statistically, SOS values were significantly different ($p < 0.0005$).

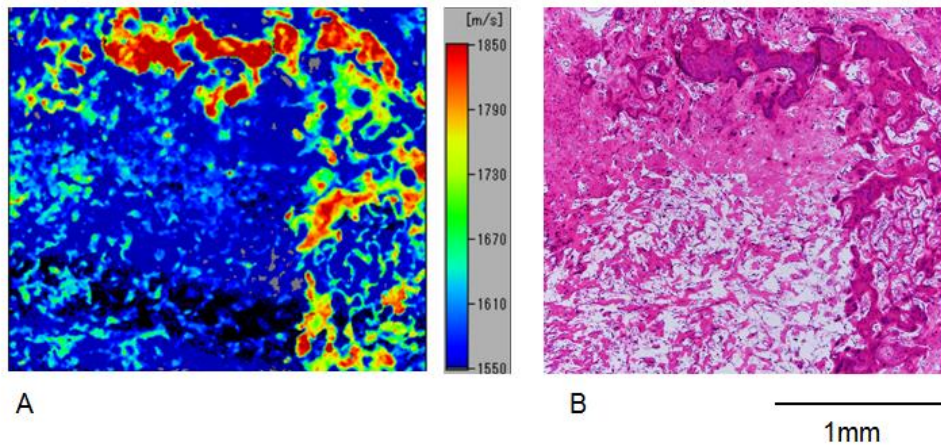


Figure 10. Osteosarcoma creating osteoid

Calcification is observed in various areas of irregularly shaped osteoid bones. The SOS image shows irregularly highly elevated ossified spaces within slightly elevated osteoid bones. A; SOS image, B; HE image

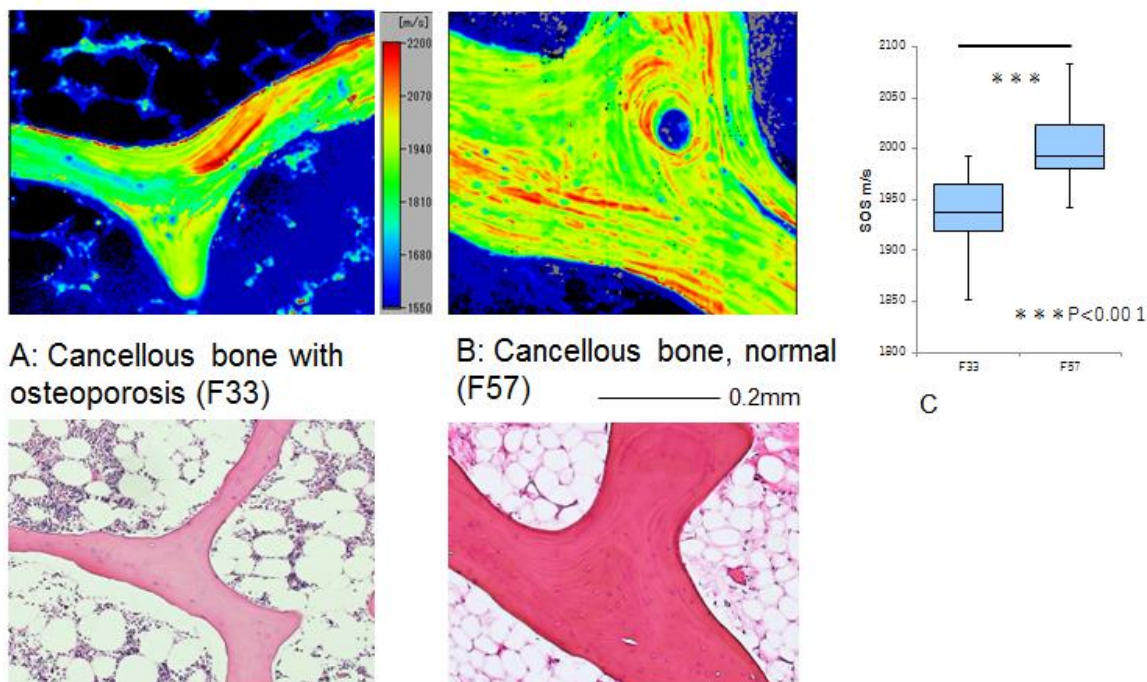


Figure 11. Comparison of speed-of-sound (SOS) values of the trabecular bone between osteoporotic and healthy bones

A, Osteoporosis after a prolonged steroid therapy (30-year-old woman); B, Healthy trabecular bone (57-year-old woman); C, Box plot of SOS values. An osteoporotic trabecula (A) is thin and displays a sparse collagen fiber, whereas a normal trabecula (B) has rich collagen fibers with high SOS values. Statistically, SOS values of these two trabeculae have significant differences (C). The box plot shows the median (horizontal line) and interquartile range. Vertical bars indicate the 5th and 95th percentiles.

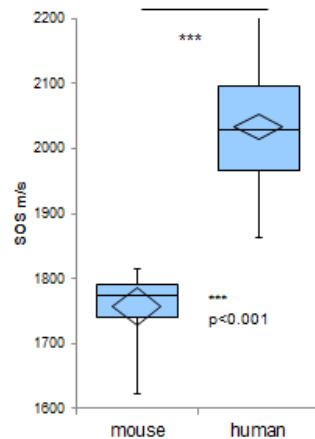


Figure 12. Comparison of the trabecular bones between mice and humans

The box plot compares SOS values between mouse and human trabecular bones. The mean values show significant differences between them ($p < 0.001$). The box plot shows the means (diamond), medians (horizontal line), and interquartile ranges. Vertical bars indicate the 5th and 95th percentiles.

COMPARISON OF TRABECULAR BONES BETWEEN MICE AND HUMANS

The trabecular bones of humans are thicker than those of mice. The mean SOS values of human

trabecular bones were significantly greater (2034.0 ± 80.2 m/s, $n = 65$ from 10 different cases) than those of mice (1757 ± 52.8 m/s, $n = 15$ from two cases) ($p < 0.001$) (Figure 12).

Discussion

The present study showed that the resolution of SOS images was similar to that of LM images, and the distinct SOS values of the bone, cartilage, and surrounding connective tissues were recognized.

Using the mean values of SOS, the organs of the mouse musculoskeletal system were divided into three groups. The lowest group included the adipose tissue, bone marrow, calcified cartilage, and nucleus pulposus. The former two are rich in lipids and are lost in tissue processing, and the latter two are proteoglycan-rich cartilages, which efficiently bind with water.

The calcified cartilage is a cartilaginous border connecting to the bone, where chondrocytes secrete matrix vesicles rich in calcium and phosphate ions^{16,17}. Moreover, this is the region where the avascular cartilaginous tissue replaces the marrow cavity and bone. Endothelial cell invasion is accompanied by proteolytic rearrangement of the cartilage matrix with metalloproteases¹⁸.

The nucleus pulposus comprises water, type II collagen, chondrocyte-like cells, and proteoglycans. This unique composite allows the nucleus pulposus to be elastic and flexible under stress forces and absorb compression¹⁹.

Sound waves did not return from the tissue surface but passed through the section of the lowest group, as in water.

The highest group comprised the vertebral disc and meniscus of fibrocartilages, rich in dense collagen bundles. In this study, collagen density and arrangement most affected the SOS values.

The intermediate group included hyaline cartilages of the meniscus and joint, osteoid, skeletal muscles, cortical and trabecular bones, and ligaments. The decalcifying procedure reduced the values of calcified bones to the ligament level, which consists of dense collagenous fibers. The osteoid, articular, and meniscus cartilages showed slightly lower values than the decalcified bones. The osteoid is an unmineralized bone and consists of type I collagen and ground substance. Skeletal muscles presented a wide variation of SOS values, with causes that depend on the direction of muscle fibers. Fibers in the longitudinal cut were higher, whereas those in the lateral cut were lower.

In humans, various orthopedic diseases displayed characteristic SOS images. Regarding fundamental differences from the mouse bone, the human trabecular bone was thicker than the mouse and showed much higher SOS values. Compared with

fibrocartilage of the periosteum, human trabecular bone showed no lower SOS values, as shown in Fig. 7. In the human musculoskeletal system, the trabecular bone ranked among the highest group in this study.

In osteoporosis, the trabecular bone becomes thin with lower SOS, indicating lesser stiffness to cause fractures. Comparison of woven and lamellar bones revealed that woven bones with lower SOS had lesser stiffness to fracture, as observed in fibrous dysplasia and osteosarcoma.

In bone fracture repair, granulation tissue is replaced by soft callus and progressively changed to more rigid and mineralized callus¹². SOS values discriminate these components and show this repairing process in Fig. 6.

Intramembranous bone formation was detected by the alteration of SOS values, as seen in Figure 8. The trabecular bone occurs from the connective tissues with an abrupt increase in SOS values. The regenerating process of bone fractures was monitored using SOS images, in which the granulation tissues transformed into calli in osteoids to grow a new mineralized bone. The stiffness increased in phases, which appeared in SOS values.

In the field of LM, several staining methods have been developed for discriminating tissue components and the functional status of the skeletal system. Gaytan¹ reported that the following requirements must be satisfied to overview the microstructure and functional characteristics of

musculoskeletal organs: (i) a clear distinction among the cartilages, fibrous collagenous tissues, and bones; (ii) a clear differentiation between uncalcified and calcified tissues; (iii) the identification of general bone structure (i.e., woven vs. lamellar); (iv) the discrimination of intramembranous bone formation versus endochondral ossification; and (v) the identification and characterization of bone cells. A single general staining method fulfilling all these requirements was not available yet.

In this study of SAM, the following results were obtained fulfilling (i)-(iv), except (v):

1. SOS images differentiated the osteoids, bones, cartilages, ligaments, and other connective tissues using decalcified FFPE sections. Fibrous-rich portions presented higher SOS values. Bone matrix components rich in proteoglycans showed lower SOS values.
2. The resolution of SOS images was comparable to LM images to identify each musculoskeletal component that showed characteristic SOS values.
3. SOS imaging helped differentiate and evaluate bone fracture recovery status, ossification process from the membrane or cartilages, bone's metabolic or degenerative status, and neoplastic bone disease characteristics.
4. The intra-articular spaces, cartilages, and facing ligaments have almost the same SOS values in the otherwise similar stiffness.

Compared to LM, SAM observation has advantages and disadvantages (Table 3).

Table 3: Differences between scanning acoustic microscopy (SAM) and light microscopy (LM)

	SAM	LM
Images	Digital	Analog
Staining	Needless	Essential
Mechanical function	Stiffness, viscosity	Undetectable
Section, thickness	Flat, about 10 μm	Flat, wide range
Observation area	Narrow, up to 4.8 mm ²	Wide range
Color change	Adjustable to the range of interest	Unavailable
Statistical analysis	Easy	Possible

The first advantage is that staining is unnecessary, which shortens the time to obtain histological images. Then, no bias is observed in the image due to variable staining results.

Second, because sound velocity correlates with stiffness, the mechanical strength of the tissue is expressed numerically, which facilitates statistical analysis.

Third, colored images can be adjusted based on the range of interest. Stiffer boney materials have higher SOS values, whereas softer cartilaginous tissues show lower SOS values. The setting range of SOS values can be adjusted in the SAM system.

Its disadvantage is the need for flat, 10-μm-thick sections. In the poorly decalcified section, the sound

is irregularly reflected on calcification; therefore, the poorly uncalcified sections are undetectable. Second, the decalcifying and tissue processing procedures alter the natural properties of the musculoskeletal tissues. Although deposited minerals disappear with lower SOS values, background fibrous components keep collagenous arrangement and density with high SOS values.

Third, the observation area with a single scan is limited to 4.8 mm² with the current equipment. Fourth, SAM is manually operated to obtain accurate sound waves; therefore, learning the detailed skills takes time.

Several methods have been used to visualize the stiffness of biological tissues, including elastography, optical coherence elastography, and micro-computed tomography. Elastography uses ultrasound²⁰ or magnetic resonance²¹ to measure the strain or displacement of tissues when subjected to an external force or vibration.

Optical coherence elastography uses optical coherence tomography to measure the propagation of mechanical waves in tissues²². Tissue stiffness is associated with speed and wave attenuation.

Micro-CT uses X-rays to obtain high-resolution three-dimensional images of tissues and their internal structures²³. Tissue stiffness can be estimated by measuring its deformation under compression or tension. The above methods need special instruments, so precise histological comparison is difficult. Other methods, including hardness tests, nanoindentation, and atomic force microscopy, have been used to measure the stiffness of microscopically small tissues.

The hardness test evaluates the hardness of metal materials by pressing a pyramid-shaped or spherical indenter into the sample and calculating it based on the size or depth of indentation²⁴. Nanoindentation measures small regions' hardness and elastic modulus by applying a load to the sample with a nanometer-level indenter and obtaining the stress-strain curve from deformation and load²⁵ using an indentation device with a microscope.

Atomic force microscopy measures surface topography and physical properties of samples by detecting the interatomic force acting on the cantilever tip that is brought close to the sample surface²⁶. Preparing samples using these methods takes time and effort or requires expensive instruments.

The SAM uses routine histological samples of approximately 10- μ m-thick sections, which need no special sample preparation, and information obtained on mechanical stiffness directly corresponds to the histological structure. Although not discussed in this study, SAM measurements also provide information on the attenuation of sound passing through these sections^{7,27}. Sound attenuation is significantly correlated with tissue viscosity, i.e., the higher the tissue viscosity, the greater the loss of energy, another mechanical property.

Conclusions

Numerical stiffness data of SAM, which cannot be determined with LM, will be used for the functional evaluation and diagnosis of bone diseases. Decalcified FFPE sections can provide important information about the structures and functions of the musculoskeletal system by SAM.

Conflicts of Interest

KM received supporting fees for attending meetings from Honda Electronics. TI has no conflicts of interest to declare.

Funding

No funding was received.

Acknowledgments

The authors acknowledged Drs. Yuki Egawa and Toshiaki Moriki at Shizuoka City Hospital and Akikazu Endo at the Division of Hospital Pathology of Hamamatsu University School of Medicine for the sample preparation. Drs. Kanna Yamashita, Michio Fujie, and Toshi Nagata of the Department of Health Science, Hamamatsu University School of Medicine provided the research facilities for this study.

References

1. Gaytan F, Morales C, Reymundo C, Tena-Sempere M. A novel RGB-trichrome staining method for routine histological analysis of musculoskeletal tissues. *Sci Rep.* 2020;10(1):1-13. doi:10.1038/s41598-020-74031-x
2. Ralis Z, Watkins G. Modified tetrachrome method for osteoid and defectively mineralized bone in paraffin sections. *Biotech Histochem.* 1992;67:339-345. doi:10.3109/10520299209110046
3. Yoshiki S. A simple histological method for identification of osteoid matrix in decalcified bone. *Stain Technol.* 1973;48:233-238. doi:10.3109/10520297309116630
4. Lemons R, Quate CF. Acoustic microscope—scanning version. *Appl Phys Lett.* 1974;24(4):163-165. doi:https://doi.org/10.1063/1.1655136
5. Miura K, Mineta H. Histological evaluation of thyroid lesions using a scanning acoustic microscope. *Pathol Lab Med Int.* 2014;6:1-9.
6. Miura K. Application of Scanning Acoustic Microscopy to Pathological Diagnosis. In: Stanciu SG, ed. *Microscopy and Analysis.* Intech; 2016:381-403. doi:10.5772/63405
7. Saijo Y. Recent Applications of Acoustic Microscopy for Quantitative Measurement of Acoustic Properties of Soft Tissues. In: Mamou J, Oelze M, eds. *Quantitative Ultrasound in Soft Tissues.* Springer; 2013:291–313. doi:10.1007/978-94-007-6952-6_12
8. Saijo Y. Acoustic microscopy: latest developments and applications. *Imaging Med.* 2009;1(1):47-63. doi:http://dx.doi.org/10.2217/iim.09.8
9. Azhari H. Appendix A: Typical Acoustic Properties of Tissues. *Basics Biomed Ultrasound Eng.* Published online 2010:313-314. doi:10.1002/9780470561478.app1
10. Raum K. Microelastic imaging of bone. *IEEE Trans Ultrason Ferroelectr Freq Control.* 2008;55(7):1417-1431. doi:10.1109/TUFFC.2008.817
11. Granke M, Gourrier A, Rupin F, et al. Microfibril Orientation Dominates the Microelastic Properties of Human Bone Tissue at the Lamellar Length Scale. *PLoS One.* 2013;8(3):1-11. doi:10.1371/journal.pone.0058043
12. Casanova M, Schindeler A, Little D, Müller R, Schneider P. Quantitative phenotyping of bone fracture repair: a review. *Bonekey Rep.* 2014;3(JULY):1-8. doi:10.1038/bonekey.2014.45
13. Miura K, Yamamoto S. Histological imaging from speed-of-sound through tissues by scanning acoustic microscopy (SAM). *Protoc Exch.* Published online 2013. doi:10.1038/protex.2013.040
14. Tamura K, Ito K, Yoshida S, Mamou J, Miura K, Yamamoto S. Alteration of speed-of-sound by fixatives and tissue processing methods in scanning acoustic microscopy. *Front Phys.* 2023;11. doi:10.3389/fphy.2023.1060296
15. Hozumi N, Yamashita R, Lee CK, et al. Time-frequency analysis for pulse driven ultrasonic microscopy for biological tissue characterization. In: *Ultrasonics.* ; 2004:717-722. doi:10.1016/j.ultras.2003.11.005
16. Wang W, Ye R, Xie W, et al. Roles of the calcified cartilage layer and its tissue engineering reconstruction in osteoarthritis treatment. *Front Bioeng Biotechnol.* 2022;10(August):1-12. doi:10.3389/fbioe.2022.911281
17. Hasegawa T, Hongo H, Yamamoto T, et al. Matrix Vesicle-Mediated Mineralization and Osteocytic Regulation of Bone Mineralization. *Int J Mol Sci.* 2022;23(17). doi:10.3390/ijms23179941
18. Blumer MJF. Bone tissue and histological and molecular events during development of the long bones. *Ann Anat.* 2021;235:151704. doi:10.1016/j.aanat.2021.151704
19. Cicco FL De, Willhuber GOC. *Nucleus Pulposus Herniation.* StatPearls Publishing; 2023.
20. DeWall R. *Ultrasound Elastography: Principles, Techniques, and Clinical Applications.* *Crit Rev Biomed Eng.* 2013;41(1):1-19.
21. Manduca A, Bayly P V., Ehman RL, et al. MR elastography: Principles, guidelines, and terminology. *Magn Reson Med.* 2021;85(5):2377-2390. doi:10.1002/mrm.28627
22. Feng X, Li GY, Ramier A, Eltony AM, Yun SH. In vivo stiffness measurement of epidermis, dermis, and hypodermis using broadband Rayleigh-wave optical coherence elastography. *Acta Biomater.* 2022;146:295-305. doi:10.1016/j.actbio.2022.04.030
23. El-Gizawy AS, Ma X, Pfeiffer F, Schiffbauer JD, Selly T. Characterization of Microarchitectures, Stiffness and Strength of Human Trabecular Bone Using Micro-Computed Tomography (Micro-CT) Scans. *BioMed.* 2023;3(1):89-100. doi:10.3390/biomed3010007
24. Clarebrough L, Hargreaves M. Hardness testing of metallic materials. 1959;(February):1-3. https://www.researchgate.net/publication/349548712
25. Qian L, Zhao H. Nanoindentation of soft biological materials. *Micromachines.* 2018;9(12). doi:10.3390/mi9120654

26. Hiesgen R, Friedrich KA. Atomic force microscopy. *PEM Fuel Cell Diagnostic Tools*. 2011;(May 2017):395-421. doi:10.4011/shikizai.93.321
27. Miura K, Fukushi Y. Scanning acoustic microscopy imaging of cellular structural and mechanical alterations from external stimuli. *Heliyon*. 2021;7(8):e07847. doi:10.1016/j.heliyon.2021.e07847